

Chiral Lemniscate Formation in Magnetic Field Controlled Topological Fluid Flows

Matt Jellicoe, Zoe Gardner, Amjad E. H. Alotaibi, Kaylee E. Shoemaker, James M. Scott, Shiliang Wang, Badriah M. Alotaibi, Xuan Luo, Clarence Chuah, Christopher T. Gibson, Shan He, Kasturi Vimalanathan, Jason R. Gascooke, Xianjue Chen, Alison Rodger, Han Huang, Scott J. Dalgarno, Elsa Antunes, Gregory A. Weiss, Qin Li, Jamie S. Quinton, and Colin L. Raston*

High shear spinning top (ST) typhoon-like fluid flow in a rapidly rotating inclined tube within a vortex fluidic device (VFD) approaches homochirality throughout the liquid with toroids of bundled single-walled carbon nanotubes (SWCNTs) twisted into stable chiral lemniscates (in the shape of Figure 8s), predominantly as the *R*- or *S*-structures, for the tube rotating clockwise (CW) or counterclockwise (CCW). However, this is impacted by the Earth's magnetic field (B_E). Theory predicts 1–20 MPa pressure for their formation, with their absolute chirality determined from scanning electron microscopy (SEM) and atomic force microscopy (AFM) images. Thus, the resultant lemniscate structures establish the absolute chirality of the inner and outer components of the ST flow. These chiral flows and lemniscates can be flipped to the opposite chirality by changing the orientation of the tube relative to the inclination angle of B_E , by moving the geographical location. Special conditions prevail where the tangential angle of the outer and inner flow of the ST becomes periodically aligned with B_E , which respectively dramatically reduce the formation of toroids (and thus lemniscates) and formation of lemniscates from the toroids formed by the double-helical (DH) flow generated by side wall Coriolis forces and Faraday waves.

1. Introduction

Selective formation of chiral nanomaterials has emerging technological prospects with the chiral induction imparted by circularly polarised light.^[1–9] An alternative approach for chiral induction in the absence of chiral auxiliary agents is to use chiral fluid flow. Chiral lift forces are parallel to the shear plane in a Taylor–Couette cell, whereas chiral-specific forces act perpendicular to the shear plane in other systems.^[10] Fluid flow discriminating between objects of opposite chirality was originally conceived by Howard et al.^[11] Even simple stirring can be effective in competing with chiral chemical induction but this requires the introduction of a chiral dopant.^[12] A challenge is to impart chirality without adding molecular chirality to initiate and control the process, and this is achieved in the present study in forming chiral lemniscates (Figure 8s) comprised of bundled

M. Jellicoe, Z. Gardner, A. E. H. Alotaibi, B. M. Alotaibi, X. Luo, C. Chuah, C. T. Gibson, S. He, K. Vimalanathan, J. R. Gascooke, J. S. Quinton, C. L. Raston

Flinders Institute for Nanoscale Science and Technology

College of Science and Engineering

Flinders University

Bedford Park, SA 5042, Australia

E-mail: colin.raston@flinders.edu.au

K. E. Shoemaker, G. A. Weiss

Department of Chemistry

University of California

Irvine, CA 92697-2025, USA

J. M. Scott, Q. Li

Queensland Quantum and Advanced Technology Research Institute

Griffith University

Nathan, QLD 4111, Australia

J. M. Scott, Q. Li

School of Engineering and Built Environment

Griffith University

Nathan, QLD 4111, Australia

S. Wang

School of Physics

Central South University

Changsha 410083, P. R. China

C. T. Gibson

Flinders Microscopy and Microanalysis

College of Science and Engineering

Flinders University

Bedford Park, SA 5042, Australia

S. He

School of Food and Pharmacy

Zhejiang Ocean University

Zhoushan, Zhejiang 316022, P. R. China

The ORCID identification number(s) for the author(s) of this article can be found under <https://doi.org/10.1002/sml.202409807>

© 2025 The Author(s). Small published by Wiley-VCH GmbH. This is an open access article under the terms of the [Creative Commons](#)

[Attribution-NonCommercial-NoDerivs](#) License, which permits use and distribution in any medium, provided the original work is properly cited, the use is non-commercial and no modifications or adaptations are made.

DOI: 10.1002/sml.202409807

SWCNTs. Fluid flow chiral induction at length scales down to those of molecules is fundamentally important in separation science,^[13,14] with recent advances in understanding this at such dimensionality.^[15]

Determining the nature of fluid flow down to nanometre (nm) dimensions can provide insight into developing flow devices for chiral discrimination as part of the toolbox for separating chiral objects, as well as preparing material of specific chirality. The vortex fluidic device (VFD) is a thin film microfluidic platform with a diversity of applications in biological, chemical, and materials processing,^[16–22] depending on the induced mechanical energy which is tuneable by varying the rotational speed, ω , and tilt angle, θ , typically using a 20 mm diameter quartz tube.^[16,17] High shear micron/submicron topological fluid flows occur in the VFD, **Figure 1a**, which have been molded using crystallizations and molecular “drilling” strategies, with immiscible liquids being mixed down to the molecular level.^[16,17] They are the spinning top (ST) typhoon-like topological flow, arising from Coriolis forces from the hemispherical base of the tube, and double helical flow (DH) generated by Faraday waves and the Coriolis forces from the side walls of the tube.^[16,17]

We hypothesized that chiral lift forces present internally in ST flow in the VFD can generate material of one specific chirality, assuming that this fluid flow is homochiral for a particular rotation direction of the tube, which is then reversed when the tube is rotated in the opposite direction. For this, we focused on attempting to twist toroids of assembled single-walled carbon nanotubes (SWCNTs) from an immiscible mixture of water and an aromatic solvent, **Figure 1b**, having observed some lemniscate (**Figure of 8**) structures for a mixture of water and toluene.^[22] We found that left- or right-handed lemniscates (*S*- and *R*-handed respectively), form in an immiscible mixture of water and *m*-xylene, **Figure 1b,c**, which is mechanistically understood by a twisting effect as a toroid is forced through a ST. Toroids of SWCNTs rapidly form at the interface of the liquid and the surface of the

tube, at the base of the DH flows, as previously established, with the ability to control their diameter, depending on the nature of the solvent and the rotational speed.^[21] These toroids can experience a lift force normal to the surface of the tube, as the liquid rises in forming a right-handed or left-handed inner ST fluid flow, which then generate *R*- or *S*-lemniscates respectively; the corresponding outer ST flow is left-handed and right-handed respectively. Surprisingly the observed behavior appears to depend upon the orientation of the tube with respect to the Earth's magnetic field, even though the field is weak ($\approx 50 \mu\text{T}$). This implies that charged particles from high dissociation of the water within the ST flow experience forces from moving in the magnetic field, and these are not insignificant when compared with the Coriolis force. From a processing perspective, the Earth's magnetic field appears to alter the diameter of the ST. Proof of the effect of the Earth's magnetic field involved i) VFD processing at different geographical locations in the northern and southern hemispheres, where the inclination angles of the Earth's magnetic field are different, ii) molecular drilling around the compass settings by ST and DH flows into thin films of polymer lining the inner surface of the VFD tube, which also established orientation of the tube where the tangential vector of the outer and inner flows ST flows periodically align with the Earth's magnetic field, and similarly iii) shear stress induced C_{60} crystallization from an immiscible mixture of toluene and water, as a desolvation effect, as previously established, albeit prior to the realization of the effect of the Earth's magnetic field relative to the orientation of the rotating tube in the VFD.^[16–18]

Substantial efforts have been devoted to achieving selective control of chirality in nanomaterials.^[1–9] More promising avenues to impart chirality, in general, can be found in the flow of liquid in magnetic fields,^[23] with magnetic fields affecting rates and yields of chemical reactions *in vitro*.^[24,25] The influence of the Earth's weak magnetic field on molecular behavior is found in Nature. For example, directional and positional information are offered through magnetic-sensitive cryptochromes that migratory birds use to traverse the world.^[26] However, because the Earth's magnetic field is inherently weak, its impact on fluid flow, as established herein, is surprising, as is controlling processing outcomes in different ways depending on the choice of geographical location.

2. Results and Discussion

2.1. Synthesis of *R*- and *S*-Lemniscates

Initially, suspensions of SWCNTs in aromatic solvents at 0.1 mg mL^{-1} , as optimized for preparing toroids of SWCNTs in the VFD exclusively,^[21,22,27] were mixed with an equivalent volume of water in a tube rotating clockwise (CW) at different rotational speeds, ω , for 1 h, with the tube facing magnetic south (S) at Flinders University (FU). At the time the significance of this orientation was not apparent. The choice of solvent and solvent mixture to form the lemniscates was systematically explored, with a 1:1 mixture of *m*-xylene and water being effective at $\omega = 7750 \text{ rpm}$, with the tube tilt angle $\theta = 45^\circ$, which is the uniquely optimal angle for most applications of the VFD.^[16–22] Other aromatic solvents, toluene and *o*-xylene, and *p*-xylene,^[21] favored predominantly the formation of the toroids in the

X. Chen
School of Environmental and Life Sciences
The University of Newcastle
Callaghan, NSW 2308, Australia
A. Rodger
Research School of Chemistry
Australian National University
ACT 2601, Australia
H. Huang
School of Advanced Manufacturing
Sun Yat-sen University
Shenzhen 518107, P. R. China
S. J. Dalgarno
Institute of Chemical Sciences
Heriot-Watt University
Riccarton, Edinburgh, Scotland EH14 4AS, UK
E. Antunes
College of Science and Engineering
James Cook University
Douglas, Townsville, QLD 4811, Australia
J. S. Quinton
School of Food Technology and Natural Sciences
Locked Bag 11222
Massey University
Palmerston North 4442, New Zealand

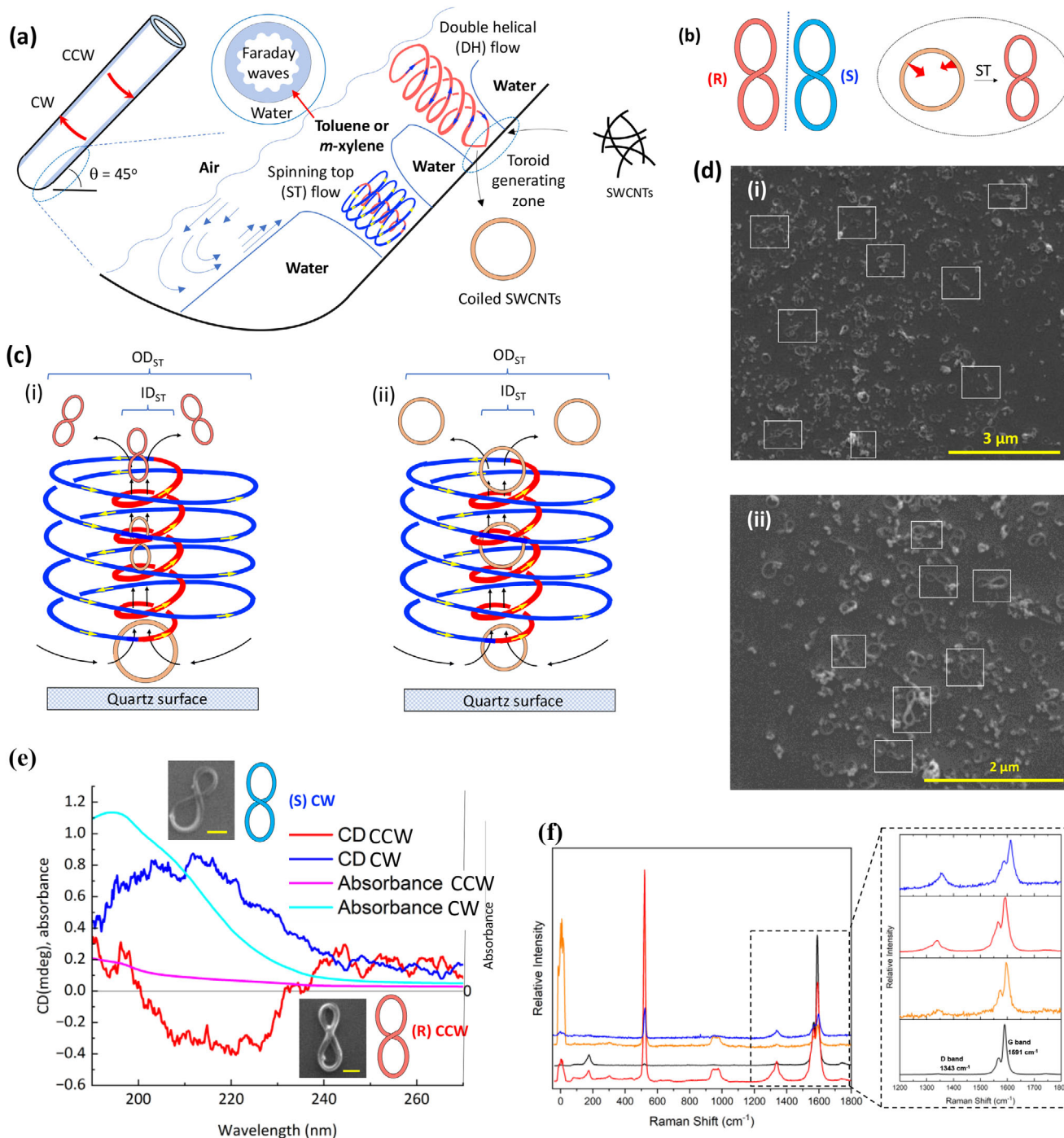


Figure 1. Synthesis and characterisation of chiral lemniscates. Schematic of a) the formation of toroids of coiled SWCNTs in the vortex fluidic device (VFD) at the base of double helical (DH) topological fluid flow generated by Faraday wave eddies and tube side wall Coriolis forces, and spinning top (ST) (typhoon like) topological fluid flow generated by Coriolis forces at the hemispherical base of the tube tilted at $\theta = 45^\circ$.^[16,17,21] b) R- and S-lemniscates (Figure of 8s) from twisting of the toroids in a), and c) the proposed mechanism of formation of lemniscates when the toroids are forced vertically through the core of the ST, with R-fluid flow resulting in R-lemniscates, (i), and smaller toroids passing through essentially unrestricted, (ii). OD indicates outer and ID indicates inner diameter of the ST. d) SEM images of (i) S- and (ii) R-lemniscates formed at Flinders University (FU) in a 20 mm OD quartz tube (17.5 mm ID, 18.5 cm in length) with a hemispherical base, facing magnetic south, rotating clockwise (CW) and counter clockwise (CCW) respectively, $\omega = 7750$ rpm, $\theta = 45^\circ$. e) Circular dichroism spectra (in millidegrees) and absorbance of CCW and CW lemniscates in (d) in a 1 cm path length 4 mm wide (black quartz masked) cuvette. Spectra are an average of 9 accumulations at 100 nm min⁻¹, 2 s digital integration time and 2 nm bandwidth. Samples were dispersed in 1% SDS, and were inverted to resuspend the samples between each accumulation. Spectra include a component of scattering, so they have not been zeroed or adjusted for concentration. Inset of SEM images of individual lemniscates, scale bar 100 nm. f) Raman spectra of as-received SWCNTs (black), toroids (orange), R- (red) and S- (blue) lemniscates formed in (d). Inset shows a zoomed in 1200–1800 cm⁻¹ region with the assigned D and G bands and the more prominent Raman shift for the S-lemniscate.

presence of an equivalent volume of water (Figures S7 and S8, Supporting Information). SEM and AFM revealed the formation of S-lemniscates, Figure 1d,e and Figures S41 and S94 (Supporting Information). Toroids of SWCNTs rapidly formed in the VFD over a few minutes²¹ which then become twisted into lemniscates over 1 h or more and are indefinitely stable. Changing the direction of rotation of the tube to counterclockwise (CCW) with the tube also facing S afforded R-lemniscates. Circular dichroism (CD) spectra were consistent with the formation of enriched S- or R-lemniscates for CW and CCW rotation (defined from the direction of looking down the tube from the open to the closed end) respectively, Figure 1e. Some differences in the CD spectra for enriched S- or R-lemniscates may arise from differences in fluid dynamic response and the nature of the associated forces involved in twisting the first-formed toroids into lemniscates. Indeed, such response is reflected in CCW rotation resulting in $\approx 15\%$ of the toroids being converted to lemniscates over 4 h, whereas for CW rotation only, $\approx 5\%$ were converted for the same processing time, as determined from SEM images. The difference in conversion was consistently the same for a number of different quartz tubes housed in the VFD, which suggests that any distortions in the tube are unlikely to be responsible for the difference. Instead, perhaps the Earth's magnetic field, B_E , is responsible for the observed difference. To test this, we repeated the same CW and CCW experiments for the tube facing N, W, and E, with the results summarised in Figure 2a and Section 2.1.1.4.1 (Supporting Information). There is a switch in chirality of the lemniscates produced for CW and CCW rotations with the tube facing W relative to facing E, and for CW N, the processed sample had a limited number of assembled structures of SWCNTs, whereas, for CCW N, toroids were present, with low amounts of lemniscates. Raman spectra showed a significant increase in strain on forming the lemniscates over the toroids, and in turn over the as-received SWCNTs, Figure 1f,^[25] with an increase in the I_D/I_G ratio.^[28] This is consistent with significant compression and elongation of carbon bonds in the lemniscates, and interestingly there is a difference in the Raman spectra between R- and S-lemniscates formed for the tube facing S and rotated CCW and CW, respectively, with that of the R-lemniscates being shifted to higher energy, where the percent conversion of the toroids to lemniscates is higher, reflecting different fluid dynamic responses by the SWCNTs impacted by B_E . Based on the radial breathing mode (RBM), the toroids and lemniscates are comprised of both metallic and semiconducting nanotubes, Section 2.1.3 (Supporting Information). The larger diameter toroids, $\approx 400\text{--}500$ nm, become twisted relative to the smaller diameter toroids, $\approx 180\text{--}340$ nm, which is consistent with the larger toroids being spatially constricted in forming lemniscates as they are forced through the ST, and less so for the smaller toroids, Figure 1. The thickness of the toroids, which relates to the number of turns of SWCNTs from one or more carbon nanotubes, is observed to vary but there is no apparent preferential twisting of the thinner (and larger) toroids into lemniscates. The percent conversion of the toroids into enriched R- or S-lemniscates, or a mixture of them varies from as high as $\approx 15\%$ down to $<1\%$, as determined from SEM images.

Given the effect of B_E on forming lemniscates, and indeed the toroids, we studied the same processing conditions at two other locations in the southern hemisphere, namely Griffith University (GU) and James Cook University (JCU), where the in-

clination angles of B_E are $+57^\circ 43'$ and $+48^\circ 28'$ respectively, much lower than that at FU, at $+67^\circ$. The outcome for GU is distinctly different to that at FU, and different again to that at JCU, Figure 2a–c and Sections 2.1.1.4.2 and 2.1.1.4.3 (Supporting Information). Samples processed CW and CCW rotations at GU which are devoid of lemniscates are for the tube facing W, albeit with a reversal of the direction of rotation affording toroids versus no organized nanostructures. Also noteworthy is that all CW and CCW rotations for the other three compass settings afford R- and S-lemniscates, respectively. The findings at JCU are similar to those at GU, but with the direction for forming toroids only, and no organized nanostructures are now observed when the VFD is oriented toward E. In contrast, for similar experiments in the northern hemisphere at the University of California, Irvine (UCI) and Heriot-Watt University (H-WU), where the inclination angles are $-58^\circ 37'$ and $-69^\circ 49'$ respectively, mixtures of S- and R-lemniscates form, except for CW W and CCW S at H-WU, which preferentially result in R- and S-lemniscates, respectively, and CCW W at UCI where no organized nanostructures were evident, Figure 2d,e and Sections 2.1.1.4.4 and 2.1.1.4.5 (Supporting Information). Relative geographical locations are shown in Figure 2f and inclination angles in Figure 2g. Further studies at FU at 45° tilt angle but with incremental orientational changes around the compass directions established the formation of mixtures of lemniscates at NW, SW, SE, and NE, as shown in Figure 2a. The twisting of toroids into either R- or S-lemniscates within the ST topological fluid flows occurs close to the base of the tube,^[12] Figure 2h, and implies that the inner ST flows are R- and S-homochiral, respectively. As such, the absolute chirality of the preferred lemniscate at N, S, and E, at FU, as determined by SEM and AFM, Figure 1d,e, and Sections 2.1.1.4.1 and 2.1.2 (Supporting Information), establish the absolute chirality of the internal flow in the ST, and thus the opposite absolute chirality for fluid flow peripheral of the ST. Where mixtures of R- and S-lemniscates are formed, the relative difference in energy in forming the R- or S-internal fluid flow in the STs is small, and in this article, we will demonstrate that the formation of these is impacted by the Earth's magnetic field. For this to occur the presence of charged species in the liquid is implied, most likely arising from high localized dissociation of water within the ST topological fluid flow.^[13]

2.2. Polymer “Drilling” and Fullerene C_{60} Thermal Desolvation

The effect of changing the orientation of B_E on the lateral dimensions of ST and DH flows was studied at FU by measuring the size of holes or craters formed in thin films of polysulfone cast on the inside of the VFD tube,^[16,17] for $\omega = 7750$ rpm, $\theta = 45^\circ$, Figure 3a,b. These experiments were for a mixture of toluene and water, rather than *m*-xylene and water because *m*-xylene results in the dissolution of the polymer, with only partial dissolution and reformation of the modified polymer at the polymer-liquid interface for the case of toluene.² Also noteworthy is that at this rotational speed, there is no distinction between the two immiscible phases under DH flow, and where preformed emulsions of the two immiscible liquids spontaneously demix.^[16,29] These “drilling” experiments establish that there is a dramatic change in the diameter of the holes by varying χ (compass

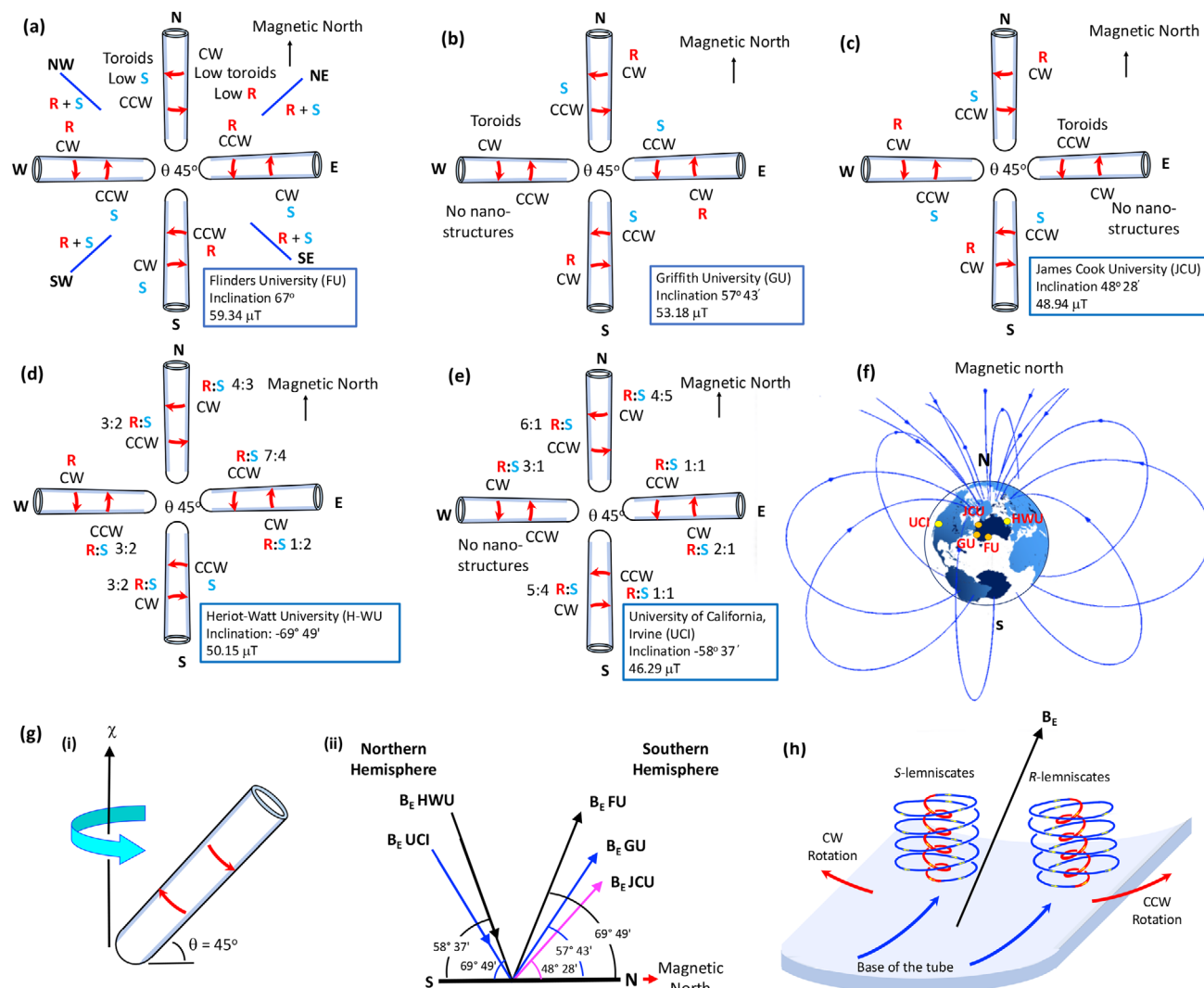


Figure 2. Earth's magnetic field dependence of formation of lemniscates. Graphical representation of processing outcomes in the VFD at different geographical locations in the southern hemisphere: a) Flinders University (FU), b) Griffith University (GU), c) James Cook University, and the northern hemisphere, d) Heriot-Watt University (H-WU), and e) the University of California, Irvine (UCI), showing inclination angle and field strength, along with their relative locations, f). (g) Graphical representation of (i) changing the orientation of the tube, χ , relative to the normal to the Earth's surface, (ii) different angles of B_E relative to magnetic north. (h) Schematic of STs of different chirality which form in the VFD in the same thin film of liquid; all experiments were in a 20 mm OD quartz tube (17.5 mm ID, 18.5 cm in length) with a hemispherical base, for ω 7750 rpm, $\theta = 45^\circ$. Determining the relative components of R- or S-lemniscates of the toroids of coiled SWCNTs used primarily SEM imaging (Sections 2.1.2–2.1.4, Supporting Information). The original experiments were done at FU then GU, and from the outcome of these experiments, the pair of samples with no lemniscates present was correctly predicted for JCU without prior knowledge of the position and direction of rotation of the tube for samples sent to FU for SEM studies.

setting), Figure 2, with the larger holes assigned to a mold of the outer diameter of ST flow and smaller holes the diameter of DH flow, Figure 3a and Section 2.2 (Supporting Information) For CW N, the holes are highly uniform, ≈ 200 nm in diameter, and are present along the length of the tube, where the axis of rotation of the outer ST flow aligns with B_E , with non-periodic Faraday waves present, in accounting for the lack of formation of toroid for this orientation of the tube. In other words, the presence and orientation of the Earth's magnetic field have facilitated the formation of the drilled holes. Other orientations show some directional alignment of the holes, suggesting that the Faraday waves here are periodic, which accounts for the SWCNTs always being coiled into

toroids.²¹ Alignment of holes is pronounced for drilling experiments for toluene alone, and also for a recently reported biphasic immiscible system where two thin films of centrifugally separated liquids of different densities move relative to each other, resulting in some loss of information on the periodicity of the holes.^[17] For the tube rotating CCW N, where the inside ST flow periodically aligns with B_E , there are large and small holes, with the outside of the ST favoring the formation of periodic Faraday waves, based on the lining up of the small holes. However, under these conditions, few lemniscates are observed to form, the product being predominantly toroids, which is consistent with the inside of the ST periodically aligning with B_E . For CW and

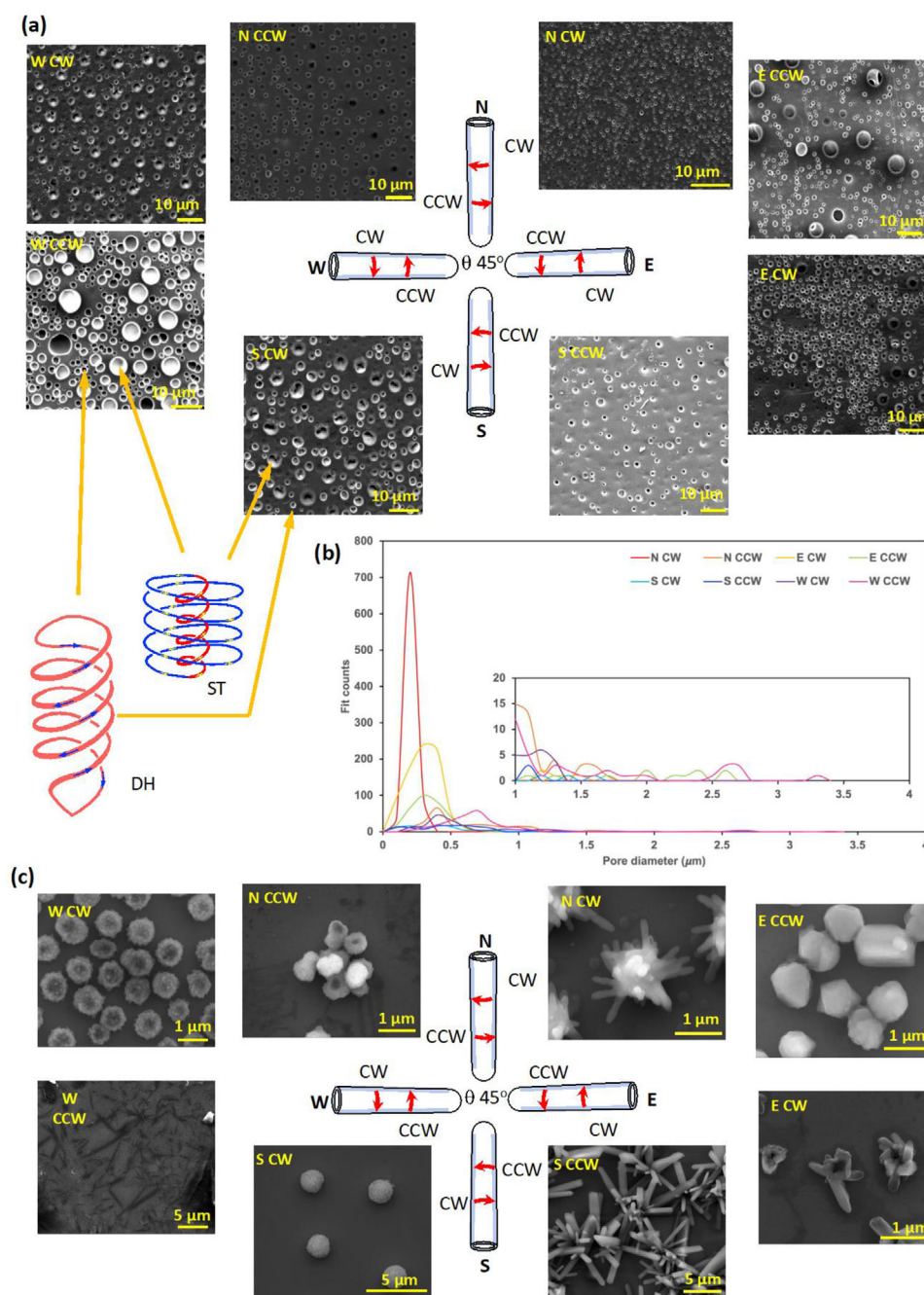


Figure 3. Earth's magnetic field topological fluid flow drilling and crystallisation effects. a) SEM images of the surface of peeled polysulfone films that were in contact with the surface of the tube during VFD processing, mid-way along the 18.5 cm quartz tube (20 mm ID, 17.5 ID) with a hemispherical base. For each experiment at different compass settings for the tube rotating CW and CCW, a film of polysulfone (≈ 20 μm thick) was prepared by evaporating a methylene chloride solution of the polysulfone (100 mg mL^{-1}) in a VFD at $\omega = 6000 \text{ rpm}$, $\theta = 5^\circ$ for 15 min.¹ A biphasic mixture of 1:1 toluene and mill-Q water (1.2 mL) was then processed in the VFD at $\omega = 7750 \text{ rpm}$, $\theta = 45^\circ$ for 15 min, followed by washing with hexane, prior to peeling the polysulfone layer; where there is a large difference in the size of the holes (pores); the smaller is ascribed as arising from DH topological fluid flow, and the larger from ST topological fluid flow.^[1,2] Details of drilling experiments at other locations along the tube and the analogous findings for experiments at UCI are detailed in Section 1.2 (Supporting Information) b) Size distribution of the holes formed for the images in (a). c) SEM images of fullerene C_{60} material crystallised during processing a 1:1 mixture of mill-Q water and a toluene solution of C_{60} below the saturation concentration (0.4 mg mL^{-1}), as a function of CW or CCW rotation, and the orientation of the aforementioned 20 mm ID quartz tube, $\omega = 7750 \text{ rpm}$, $\theta = 45^\circ$ for 30 min, with further details in Section 1.3 (Supporting Information).

CCW S, E, and W rotations, there are smaller holes that line up to varying degrees, arising from DH flows which generate toroids at their base, and non-periodic larger holes for ST flows. These ST flows form at the base of the tube and is responsible for forming lemniscates (from the initially formed DH generated toroids), as identified for each CW and CCW direction, with them all affording toroids. VFD processing in a magnetic field-free region created using three orthogonal Helmholtz coils in generating a magnetic free region, Sections 2.2.4.3 and 2.2.4.4 (Supporting Information), resulted in an increase of the overall diameter of all drilled holes, for all directions and rotations around the normal to the Earth's surface, χ , when ω is 7750 rpm. At UCI the effect of B_E on the diameter of the holes was explored, in Section 2.2.3 (Supporting Information), with the holes for ST and DH flows being of similar diameter for all χ directions. This is consistent with the formation of both toroids and R- and S-lemniscates across all directions, although for CCW W rotation no toroids or lemniscates are formed, Figure 2e. The effect of B_E on the diameter of the ST topological fluid flows implies the generation of charged species under shear stress, with an assumed higher dissociation of water in the water phase. Knowing the absolute chiralities of the lemniscates, and by inference, the absolute chiralities of the internal flow of the STs, negatively charged species are impacting the fluid flow, most likely as hydroxide ions, OH^- .

Further evidence of the effect of B_E on the fluid flow is demonstrated through processing a 1:1 mixture of water and toluene, with the toluene as a solution of fullerene C_{60} . Previous studies established that this results in the crystallization of the fullerene, despite its concentration being below saturation level, and that it is effective in casting a mold of high-shear topological fluid flows in the VFD¹ (Section 1.3.1, Supporting Information). This is thought to be due to a thermal-induced desolvation effect, as established for C_{70} processing in the VFD.^[30] Results of processing at $\omega = 7750$ rpm, analogous to the drilling experiments, are summarised in, Figure 3c and Section 2.3 (Supporting Information), with different structures being generated around the compass in a way that is largely complementary to the drilling experiments for both CW and CCW rotations, as depicted earlier in Figure 3a. CW N rotation afforded radiating aggregates of rods with the overall dimensions commensurate with the larger holes drilled on the polysulfone film, and where periodic alignment occurs on the outer part of the ST. This is consistent with thermal desolvation and aggregation of the fullerene molecules from the heating and from the interplay of B_E and the tangential vector of the negatively charged OH^- generated by the induced shear stress. CCW N rotations resulted in toroids of the fullerene with a central void ≈ 200 nm (Figure S179, Supporting Information), matching the diameter of the holes drilled in the polysulfone film. This is consistent with localized heating associated with periodic alignment of the inner ST with B_E . CW S resulted in spheroidal structures with diameters similar to those of the analogous larger ≈ 3 μm diameter holes drilled in the polysulfone film, with similar findings for CCW W. The results are consistent with the thermal desolvation of C_{60} at the base of the ST, at the interface of the liquid and the surface of the quartz tube. CCW S rotation results in ≈ 0.5 μm diameter rods with larger holes at this speed ≈ 2 μm in diameter, and this is consistent with thermal desolvation inside the ST. CW W rotation gave ≈ 0.8 μm diameter particles with roughened surfaces, but the holes drilled are much bigger at 2 μm in diameter

and the understanding of this difference is the subject of future studies. CCW E rotation resulted in crystals of C_{60} ≈ 1 μm in diameter, whereas the corresponding drilled holes are ≈ 6 μm in diameter, and presumably here the crystals form inside the ST. In contrast, for CW E rotation, fullerene crystal growth affords flower-like structures with a central void ≈ 200 nm in diameter, and the formation of this structure is likely from DH flow for which the flow tapers close to the surface of the tube, which in other solvent systems can generate cones of self-assembled C_{60} attached to the quartz tube through their tips.^[31] This is consistent with the smallest holes drilled in the polysulfone film, ≈ 0.5 μm in diameter (tapering close to the surface of the tube), with the larger holes ≈ 2.5 μm in diameter, corresponding to DH and ST flow, respectively. Nevertheless, the C_{60} crystallization establishes that B_E impacts the ST flow, depending on the orientation of B_E relative to that of the VFD tube at $\theta = 45^\circ$. In a previous study, we established that micron-sized ST topological fluid flow can provide sufficient local energy to melt elemental bismuth (m.p. 271.4 °C), which is consistent with reaching high temperatures close to the base of the ST and in its central up-lift zone, and this supports a thermal desolvation effect in forming nanomaterials of crystalline fullerenes.^[16,30] The different fullerene structures formed depending on the orientation of B_E , and without symmetrical analogs structure being formed for processing W and E is consistent with the flipping of the preferred chiral lemniscate at FU, Figure 2a. This difference may also be related to the ST not being orthogonal to the surface of the tube.

2.3. Mechanism of Formation of S- and R-Lemniscates

ST flow forms at the underside base of the tube, and when the tube is facing N at FU the direction of B_E is 22° up from the rotation axis of the tube, defined as ϕ , and as the orientation of the tube is varied around χ , ϕ increases to a maximum of 68° for the tube facing S, Figure 4a. As the tube is oriented away from N for CW rotation, where the aforementioned periodic alignment occurs for the outer ST, a mixture of R- and S-lemniscates form (NW) with R-lemniscates formed for the tube facing W, and similarly for NE in forming a mixture of R- and S-lemniscates, but for E the S-lemniscate is dominant, Figure 4b(i). For CCW rotations across these orientations, periodic alignment of B_E with the inside of the ST occurs for the tube facing N, with mixtures of R- and S-lemniscates formed for the tube facing NW and NE, with now S-lemniscates and R-lemniscates formed for W and E orientations, respectively, Figure 4b(ii).

For the SW and SE orientations, mixtures of lemniscates are formed for CW and CCW rotations, with R- and S-lemniscates formed for CCW and CW respectively, which is the reverse for the findings for W, but the same as E orientation, Figure 2a. This arises from the change in ϕ around χ , which is significantly different at GU and JCU where the inclination angle of B_E is less, Figure 4a(ii). At UCI and H-WU in the northern hemisphere, the variation in ϕ is similar to that at GU and FU respectively, but the inclination angle of B_E is directed down, opposite to the locations in the southern hemisphere, and this must affect the ability of the ST flows to preferentially form R- and S-lemniscates in the northern hemisphere. Vector analysis of the ST flows for an idealized $\phi = 90^\circ$, reveals that for the ST with the right handed

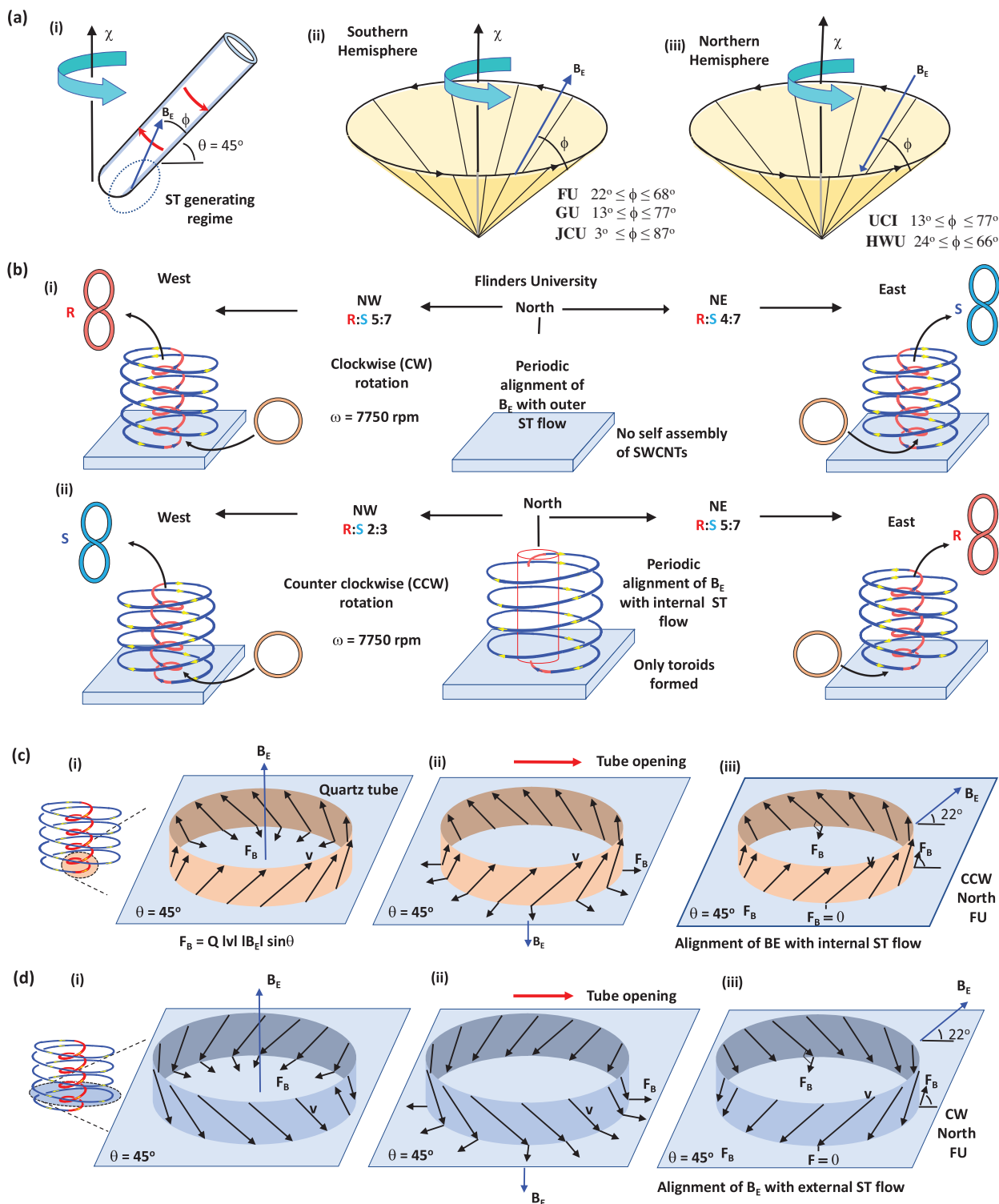


Figure 4. Geographical dependence of the Earth's magnetic field. a) Graphical representation of (i) changing the orientation of the tube, χ , with the VFD tube facing north at FU where B_E is 22° , defined as ϕ , above the rotation axis of the tube, (ii) and (iii) changes in ϕ around χ for the different geographical locations in Figure 2, for the southern and northern hemispheres respectively. b) (i) Processing at FU showing the different outcomes in transversing W, N, and E for CW rotations, with periodic alignment of B_E with the outer flow of the ST, for the tube facing magnetic N, and (ii) similarly for CCW rotation where alignment occurs for the inner flow of the ST, with reversal of the chirality of the lemniscates for W and E directions. c) Representation of the relative forces for the inner ST flow subjected to B_E directed above or below the surface of the tube at idealized at $\phi = \pm 90^\circ$, (i) and (ii), and (iii) where B_E periodically aligns with the tangential vector for flow directed up the inner part of the ST. d) Analogous representation of the relative forces for the outside of ST fluid flow at FU, with (i) and (ii) $\phi = \pm 90^\circ$, and for (iii) with B_E periodically aligning with the fluid flow on the outer ST flow toward the surface of the tube, at FU.

internal flow, for the lift away from the surface of the tube, the force generated by B_E for moving negatively charged particles (OH^-), will decrease the internal diameter of the ST, Figure 4c(i), whereas for B_E directed below the surface of the tube, also for an idealized $\phi = 90^\circ$, the force will increase the internal diameter of the ST, Figure 4c(ii). If the take-off angle inside the ST periodically aligns with B_E , where $\phi = 22^\circ$ (tube facing N, CCW rotation at FU), the net result is that there is a fluctuation in the resulting force, which accounts for the low conversion of toroids to lemniscates, Figure 4c(iii). For the same ST, with the external flow of opposite chirality to the internal flow, the situation is the same with the net force reducing the diameter of the flow, for the idealized $\phi = 90^\circ$, Figure 4d(i), and increasing for $\phi = -90^\circ$ (northern hemisphere), Figure 4d(ii), with ϕ periodically aligning with B_E at FU for N CW rotation, Figure 4d(iii). (Further explanation of the vector analysis and induced forces associated with B_E are detailed in Figure S206, Supporting Information).

The model presented above has the inner and outer flow of the ST being forced in the same direction and is consistent with how the diameter of the ST flows change with the changing diameter of the holes drilled in the polysulfone films, and the crystallization of C_{60} , Figure 3. For example, drilling experiments at FU for the tube facing W with CW rotation gave smaller diameter holes for the ST flow than for CCW rotation, $\approx 6 \mu\text{m}$ versus $\approx 2 \mu\text{m}$; similar differences are for E and W, CW, and CCW rotations. This is reversed for S CW and CCW rotation, which is consistent with the reversal of chiralities for the generated lemniscates relative to those generated for E and W orientations of the tube. It also accounts for the periodic alignment of B_E with the outer ST flow for N CCW rotation, where all the holes are approximately the same diameter, and the periodic alignment of B_E for the outer ST flow for N CW rotations with DH flows is also present. The same also applies to the periodic alignments at GU and JCU which occur where the different alignments prevail for CW and CCW rotations, (Figure 2b,c).

2.4. Helmholtz Coil and Effects of Varying Magnetic Field

Experiments with the orientation of the VFD relative to the Earth's magnetic field varied and were crucial to identifying the influence of a magnetic field, which would ordinarily be thought to be weak and insignificant. The results presented to this point indicate that there are considerable magnetic effects. However, applying artificially created magnetic fields of adjustable intensity affords opportunities to examine the possibility of magnetically controlled processing environments within the VFD in general. Applying an external magnetic field of much greater strength than the Earth's natural magnetic field around and parallel with the rotating tube in the VFD, also afforded lemniscates, but only for the field in the lower half of the tube and with the N magnetic pole close to the base of the tube. Figure 5a. A magnetic field $\approx 0.065 \text{ T}$ was generated by a stack of 8 neodymium ring magnets. For the S pole closest to the base of the tube, CW and CCW rotations gave toroids only, Figure 5a(iii). Changing the direction of the poles of the magnet around the lower section of the VFD tube resulted in the formation of toroids and lemniscates for both CW and CCW rotations, with a 2:1 and 1:2 ratio of R-and S-lemniscates, respectively using SEM images (Figure 5a(iv)). This

is in contrast to enriched S-or R-lemniscates being formed for CW and CCW rotations, respectively, for the tube orientated in the S direction, Figure 2a. For the applied magnetic field in the upper section of the tube, toroids are formed for CW and CCW rotations for the S and N magnet poles, respectively, close to the top of the tube. While toroids of SWCNTs are not formed, the SWCNTs are sliced into small lengths, a phenomenon previously reported in the VFD,^[32] with results herein detailed in Section 2.1.1.2.1 (Supporting Information) These different outcomes establish the effect of an applied magnetic field in controlling the assembly or otherwise of SWCNTs, and support the findings on the ability of B_E to control fluid flow. This difference in the applied magnetic field versus B_E relates to the non-uniform nature of the applied field across the length scale of the VFD tube, unlike B_E . It also establishes the ability to control the processing outcomes depending on the position of the magnet poles and their position along the tube. Also noteworthy is that changing the base of the tube from a hemisphere for all of the above experiments to essentially a flat base, results in different outcomes, including slicing of the SWCNTs for either CW or CCW rotations for the S magnet pole close to the top of the tube, with no exclusive formation of either the S-or R-lemniscates, Section 2.1.1.2.2 (Supporting Information).

Given the results for the applied magnetic field aligned with B_E , we sought to investigate the outcome of processing with the tube in the VFD aligned with B_E , and where the processing is in a Helmholtz coil to negate the effect of B_E , Figure 5b. For the latter at FU, with $\omega = 7750 \text{ rpm}$ and $\theta = 45^\circ$, and N and S orientations of the tube, mixtures of S-and R-lemniscates (along with the precursor toroids) are formed for both CW and CCW rotations, consistent with situations where the ST fluid flow is not perturbed by B_E . The formation of toroids and lemniscates for N facing tubes (CW and CCW) aligned with B_E is consistent with the above periodic alignment of ST flow with the Earth's magnetic field resulting in limited nanostructures and toroids only for CW and CCW, respectively. For the tube facing S for CW and CCW rotations in the Helmholtz coil, mixtures of lemniscates are formed, in contrast to the Earth's magnetic field favoring one enantiomer over another, Figures 2 and 4.

When the rotation axis of the tube was aligned with B_E , a mixture of lemniscates or no nanostructures was observed at both FU and GU, Figure 5b. At JCU, R-and S-lemniscates were observed for CW and CCW, respectively, as for CW and CCW, for tubes facing north at JCU, noting that the difference in angle between B_E and $\theta = 45^\circ$ at this location is only $3^\circ 28'$. Processing at UCI gave chiral induction, with the chiralities opposite to that at JCU, i.e., S-and R-lemniscates for CW and CCW, respectively. While these findings are for different inclinations of the tube relative to B_E , they are consistent with a flipping of chirality of the ST fluid flow between the two hemispheres. At H-WU, R-and a mixture of R-and S-lemniscates form for CW and CCW respectively. R-and S-lemniscates were observed, for CW and CCW, respectively, for $\omega 7750 \text{ rpm}$ and $\theta 45^\circ$, and changing the orientation of the VFD tube from facing magnetic N or S gave the same specific lemniscates as for CW and CCW rotations, Figure 5b and Section 2.2, Figure S206 (Supporting Information). Use of the VFD can reverse the formation of the predominant lemniscates, demonstrated for example for W and E orientation of the tube, at FU with $\omega = 7750 \text{ rpm}$ and $\theta = 45^\circ$, and

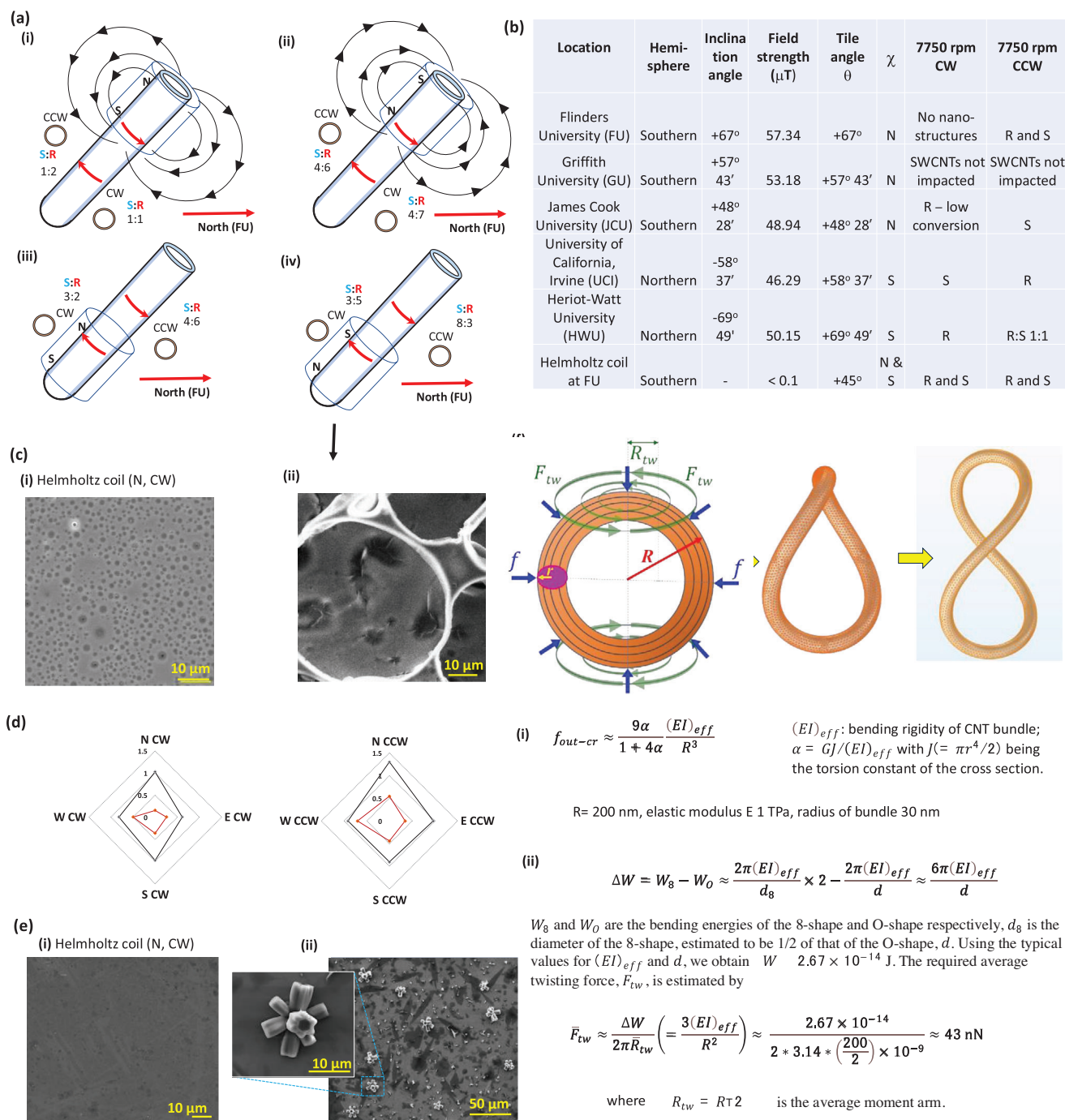


Figure 5. Helmholtz coil and different magnetic field effects for lemniscate formation. (a) Processing SWCNTs at FU using in a ≈ 0.065 T magnetic field from 8 stacked ring magnets (each OD 30 mm, ID 23 mm, thickness 8 mm) placed around the upper section of the VFD tube, with the tube facing S, (i) and (ii), forming toroids for CCW rotation with no assembled SWCNT nanostructures for CW rotations for both directions of the poles, and placed around the lower section of the tube, forming toroids for CW and CCW rotations, (iii) and (iv), or toroids and mixtures of R- and S-lemniscates for CW and CCW rotations on reversing the direction of the poles. b) Tabulation of the processing outcomes when the tilt angle of the VFD tube, θ , is parallel with the direction of B_E , for both CW and CCW rotation at $\omega = 7750$ rpm. (c) SEM images of polysulfone films (see Figure 3) taken from the mid-section of the tube after processing 1.2 mL of a 1:1 toluene at $\omega = 7750$ rpm for 10 min at $\theta = 45^\circ$, at FU. (i) N CW rotation in a Helmholtz coil, (ii) N, CW with the magnet at the base of the tube, as for (a) (iv) above. d) Average size distribution of the holes formed at (i) CW and (ii) CCW for $\omega = 7750$ rpm, $\theta = 45^\circ$, without a Helmholtz coil (red) and in a Helmholtz coil (black). e) SEM images of C_{60} particles generated in the VFD at FU as for Figure 3, (i) N CW rotation in a Helmholtz coil, (ii) N, CW rotation with the magnet at the base of the tube, as for (a) (iv) above, with other orientation outcomes in Supporting Information 1.2. f) Estimated pressure for the out-of-plane buckling of a toroid, (i), and the minimum force for twisting a toroid into a lemniscate, (ii).

this is consistent with B_E controlling the fluid flow in the VFD, Figure 3a.

Drilling experiments at FU in the Helmholtz coil gave significantly different results relative to drilling in the presence of B_E , Figure 5c,d, also confirming that B_E is affecting fluid flow. In addition, processing a 1:1 mixture of water and toluene containing dissolved C_{60} resulted in the little formation of nanostructures of the fullerene for CW and CCW N, S, E, and W rotations, confirming that the thermal desolvation effect is a result of localized heating from the B_E , forcing a change in direction of fluid flow in the ST, Figure 5e(i) and Figures S195–S202 (Supporting Information). However, the effects of B_E are not completely removed, as evidenced by some rectangular sheets, radiating octahedral prisms, and regular prisms for CW S, CCW S, and CCE E, respectively. These findings are distinctly different in the absence of the Helmholtz coil, further highlighting the impact of magnetic fields on fluid flow in the VFD. This is further confirmed by applying the aforementioned magnetic field, with now different self-assembled C_{60} outcomes, depending on the position of the stacked magnets at the top half or bottom half of the tube, and the orientation of the poles of the magnet relative to the rotation axis of the tube, Figure 5e(ii) and Figures S183–S194 (Supporting Information). For the upper positioning of the magnet with the N pole closest to the top of the tube, little fullerene material was evident, for CW and CCW N, whereas flipping the poles of the magnet results in spicular structures with holes drilled through the arms, Figure 5e(ii). Positioning the magnet at the lower half of the tube gives the same spicular structures, except for CW rotation with the S pole of the magnet close to the base of the tube, which affords 2D sheets of fullerene material, Figure S191 (Supporting Information). The effect of the applied magnetic field is complicated by its non-uniformity in orientation, strength, and location along the rotating tube.

We have also estimated the pressure required for the out-of-plane buckling of a toroid to start the twisting of a toroid into a lemniscate, which is remarkably high, ranging between 1 and 20 MPa, along with the minimum force required for twisting a toroid into a lemniscate, at ≈ 43 nN, Figure 5f(i),(ii), respectively, and Section 2.3 (Supporting Information) This alone provides insight into the high pressures and forces in the VFD, for which direct measurement in the VFD in a rotating reference frame is inherently difficult.

3. Conclusion

We have established direct and selective homochiral induction in the VFD. Depending on the dimensionality of the ST fluid flow, there are tantalizing possibilities in general for making chiral molecules, macromolecules, and materials, without the need for adding chiral auxiliary agents to induce chirality. We were unable to reverse the process of forming lemniscates by altering the processing parameters in the VFD, or indeed converting the R-isomer into the S-isomer or vice versa in the VFD. Remarkably, the absolute chirality of lemniscates is determined through inspection of the post-VFD processed material. The observations infer the dominant chirality of the topological fluid flow. This work gives insight into the origin of life, in that fluid flow coupled with magnetic fields can result in the preference of one chirality over another. The findings also highlight the potential for opti-

mizing processing outcomes by exploring the complete 3D space for applied fields $\gg B_E$ to overcome variations in B_E strength and direction which depend on geographical locations. It is important to develop systems for which the applied field is constant over the length scale of the VFD tube. Applied magnetic fields can control material processing, and chemical and biochemical transformations, driven by the increase in shear stress at the nanometre dimension, with the associated localized thermal heating potentially driving reactions and processes, which can be switched in a Helmholtz coil. The effect of B_E on controlling fluid flow implies that water is highly dissociated under shear within the ST topological fluid flow which in turn has implications for auto-base or -acid catalysis in water. Options for combining other field effects with applied B is another strategy for the VFD processing toolbox, and for more conventional micro fluidic channel-based reactors, and beyond.

Understanding the forces involved in the VFD for forming lemniscates from coiled SWCNTs, at least for the standard 20 mm OD VFD tube with a hemispherical base, is important in realizing the full potential of the device, noting that the forces involved cannot be measured directly in a rotating reference frame of the VFD. The VFD has been effective in separating proteins into preferential immiscible liquid phases,^[29] and the present work gives insight into the possibility of separating chiral molecules/macromolecules in the device. The ability of the VFD to slice SWCNTs for certain configurations with the prevailing magnetic field highlights possibilities for fully realizing the potential of the VFD for slicing carbon nanotubes without the need for in situ irradiation, which can be amplified by changing the curvature of the base of the tube, as well as using different diameter tubes.^[16,17] The findings further support the model of fluid flow in the VFD, and the ability to generate lemniscates is a way of probing the structure of fluid flow under shear, in determining its absolute chirality. This work commenced in the southern hemisphere at a mid-latitude. If the work had been performed at low latitudes (ie, close to the equator), or indeed at mid-latitude in the northern hemisphere where there was limited selectivity in preparing homochiral samples, Figure 2, discovering the induction of chirality by fluid flow would have been problematic.

Remarkably, the sensitivity of VFD processing to the Earth's magnetic field is on par with quantum sensing using molecular spin systems.^[33] Under particular operational conditions, the vortices in VFD appear “in phase” with the Earth's magnetic field, which may result in radical formation and electron transfer that are sensitive to the magnetic field. Investigations on the associations between VFD processing and other quantum phenomena are underway. We note that the metamaterial SWCNT toroids and lemniscates generated by the VFD process are potentially useful components in quantum devices for manipulating photons and electrons. In addition to its environmental benefits, by significantly simplifying nanofabrication processes, VFD processing has created novel metamaterials that have not been made before with strong potential in quantum technologies. In previous studies we have established the benefits of processing in the VFD in general, beyond materials processing into controlling chemical reactivity and selectivity, enhancing enzymatic reactions, and facilitating protein folding,^[15,18] and that it is an energy-efficient microfluidic platform. The present findings suggest that further refinements of processing in the VFD are possible from the

effect of magnetic fields, with the potential for further enhancing the green chemistry metrics of using the device.

4. Experimental Section

The VFD was a thin microfluidic processing platform housing a rapidly rotating tube tilted at $\theta = 45^\circ$, with all processing herein in the device carried out at room temperature. Unless otherwise stated, the tube was made of quartz, 20 mm OD (17.5 mm ID, 18.5 cm in length) with a hemispherical base, noting that changing the shape of the base of the tube changes the fluid flow and potentially the processing outcomes.^[2] The importance of the tilt angle being at $\theta = 45^\circ$ had been established as reproducibly optimal for a diverse range of applications of the device and was adhered to for all processing unless otherwise indicated. The choice of specific rotational speeds impacts the dimensionality and dominance of the different topological fluid flows and consequently on processing outcomes, which had been previously reported.^[1,2] All processing for generating the lemniscates at the different geographical locations was for 1 mL of a 1:1 mixture of *m*-xylene and water, the concentration of SWCNTs = 0.16 mg mL⁻¹, for a processing time of 240 min, $\omega = 7750$ rpm and $\theta = 45^\circ$. The ratio of different chirality of the lemniscates was obtained exclusively from SEM images, counting each lemniscate within the field of view. Further details of VFD processing and all other experiments, characterizations, and calculations are included in the Figure captions and the Supporting Information file.

Supporting Information

Supporting Information is available from the Wiley Online Library or from the author.

Acknowledgements

Support of this work by the Australian Research Council (DP200101105, DP200101106, and DP230100479), and the Government of South Australia is greatly acknowledged, as is the expertise, equipment, and support provided by the South Australian nodes of Microscopy Australia (MA) and the Australian National Fabrication Facility (ANFF) as an initiative under the National Collaborative Research Infrastructure Strategy (NCRIS) at Flinders Microscopy and Microanalysis.

Open access publishing facilitated by Flinders University, as part of the Wiley - Flinders University agreement via the Council of Australian University Librarians.

Conflict of Interest

The authors declare no conflict of interest.

Author Contributions

M.J., Z.G., and A.E.H.A. contributed equally to this work. C.L.R. conceived the idea, proposed the experimental design along with J.S.Q., and coordinated the research. M.J., Z.G., K.E.S., J.S., S.J.D., and E.A. processed SWCNTs, under the supervision of C.L.R., G.A.W., J.S.Q., and Q.L., with M.J. and Z.G. undertaking SEM studies. Z.G. carried out all polysulfone experiments and Fiji software analysis. A.E.H.A. carried out fullerene processing and characterization. S.W., H.H., and Q.L. developed the buckling and force model for forming lemniscates. X.C. and A.R. undertook CD studies. J.R.G. contributed to the physics and set up the Helmholtz coil with J.S.Q. for use by M.J. and Z.G. for processing SWCNTs, Z.G. for polysulfone experiments, and A.E.H.A. for processing fullerene solutions. M.J., Z.G., and A.E.H. applied ring magnets for processing SWCNTs, polysulfone experiments, and fullerene solutions. M.J. and C.T.G. carried out Raman spectroscopic studies. B.M.A., K.V., C.C., S.H., and X.L. contributed

to the development of the experiments. C.L.R. developed the model for forming the lemniscates and the understanding of chiral induction variances based on vector analysis. C.L.R., Q.L., and E.A. secured the funding. C.L.R. wrote the first draft of the manuscript. J.R.G., A.R., G.A.W., Q.L. and J.S.Q. helped revise the manuscript. All the authors contributed to comments on and revision of the manuscript.

Data Availability Statement

The data that support the findings of this study are available in the supplementary material of this article.

Keywords

asymmetric induction, chiral fluid flow, earth's magnetic field, single walled carbon nanotubes, thin film microfluidics, vortex fluids

Received: October 21, 2024

Revised: March 19, 2025

Published online: April 3, 2025

- [1] J. T. Collins, K. R. Rusimova, D. C. Hooper, H.-H. Jeong, L. Ohnutek, F. Pradaux-Caggiano, T. Verbiest, D. R. Carbery, P. Fischer, V. K. Valev, *Phys. Rev. X* **2019**, 9, 011024.
- [2] V. Soni, E. S. Bililign, S. Magkiriadou, S. Sacanna, D. Bartolo, M. J. Shelley, W. T. M. Irvine, *Nat. Phys.* **2019**, 15, 1188.
- [3] J. Ni, S. Liu, G. Hu, Y. Hu, Z. Lao, J. Li, Q. Zhang, D. Wu, S. Dong, J. Chu, C. W. Qiu, *ACS Nano* **2021**, 15, 2893.
- [4] J. K. Gansel, M. Thiel, M. S. Rill, M. Decker, K. Bade, V. Saile, G. von Freymann, S. Linden, M. Wegener, *Science* **2009**, 325, 1513.
- [5] Y. Zhao, M. A. Belkin, A. Alù, *Nat. Commun.* **2012**, 3, 870.
- [6] W. Ma, H. Kuang, L. Xu, L. Ding, C. Xu, L. Wang, N. A. Kotov, *Nat. Commun.* **2013**, 4, 2689.
- [7] C. M. Soukoulis, S. Linden, M. Wegener, *Science* **2007**, 315, 47.
- [8] R. Schreiber, N. Luong, Z. Fan, A. Kuzyk, P. C. Nickels, T. Zhang, D. M. Smith, B. Yurke, W. Kuang, A. O. Govorov, T. Liedl, *Nat. Commun.* **2013**, 4, 2948.
- [9] Y. Kim, B. Yeom, O. Arteaga, S. Jo Yoo, S.-G. Lee, J.-G. Kim, N. A. Kotov, *Nat. Mater.* **2016**, 15, 461.
- [10] T. M. Hermans, K. J. M. Bishop, P. S. Stewart, S. H. Davis, B. A. Grzybowski, *Nat. Commun.* **2015**, 6, 5640.
- [11] D. W. Howard, E. N. Lightfoot, J. O. Hirschfelder, *AIChE J.* **1976**, 22, 794.
- [12] N. Petit-Garrido, J. Claret, J. Igné's-Mullol, F. Sague's, *Nat. Commun.* **2012**, 3, 1001.
- [13] N. M. Maier, P. Franco, W. Lindner, *J. Chromatogr. A* **2001**, 906, 3.
- [14] W. H. Pirkle, T. C. Pochapsky, *Chem. Rev.* **1989**, 89, 347.
- [15] E. C. Sanders, S. R. Sen, A. A. Gelston, A. M. Santos, X. Luo, K. Bhuvan, D. Y. Tang, C. L. Raston, G. A. Weiss, *Angew. Chem., Int. Ed.* **2022**, 61, 202202021.
- [16] T. M. D. Alharbi, M. Jellicoe, X. Luo, K. Vimalanathan, I. K. Alsulami, B. S. Al Harbi, A. Igder, F. A. J. Alrashaidi, X. Chen, K. A. Stubbs, J. M. Chalker, W. Zhang, R. A. Boulous, D. B. Jones, J. S. Quinton, C. L. Raston, *Nanoscale Adv.* **2021**, 3, 3064.
- [17] M. Jellicoe, A. Igder, C. Chuah, D. B. Jones, X. Luo, K. A. Stubbs, E. M. Crawley, S. J. Pye, N. Joseph, K. Vimalanathan, Z. Gardner, D. P. Harvey, X. Chen, F. Salvemini, S. He, W. Zhang, J. M. Chalker, J. S. Quinton, Y. Tang, C. L. Raston, *Chem. Sci.* **2022**, 13, 3375.

- [18] C. Chuah, X. Luo, J. Tavakoli, Y. Tang, C. L. Raston, *Aggregate* **2024**, 5, 433.
- [19] N. Joseph, M. Mirzamani, T. Abudiyah, A. H. M. Al-Antaki, M. Jellicoe, D. P. Harvey, E. Crawley, C. Chuah, A. E. Whitten, E. P. Gilbert, S. Qian, L. He, M. Z. Michael, H. Kumari, C. L. Raston, *Nanoscale Advances* **2024**, 6, 1202.
- [20] X. Luo, W. Xing, I. Delcheva, F. A. Alrashaidi, A. Heydari, D. Palms, V. K. Truong, K. Vasilev, Z. Jia, W. Zhang, P. Su, K. Vimalanathan, A. Igder, G. A. Weiss, Y. Tang, M. MacGregor, C. L. Raston, *ACS Appl. Mater. Interfaces* **2023**, 15, 31114.
- [21] M. Jellicoe, C. T. Gibson, J. S. Quinton, C. L. Raston, *ACS Appl. Nano Mater.* **2022**, 5, 11586.
- [22] K. Vimalanathan, X. Chen, C. L. Raston, *Chem. Commun.* **2014**, 50, 11295.
- [23] A. Hayat, J. P. B. Mueller, F. Capasso, *Proc. Acad. Nat. Sc* **2015**, 112, 13190.
- [24] W. E. Steiner, T. Ulrich, *Chem. Rev.* **1989**, 89, 51.
- [25] B. Brocklehurst, *Chem. Soc. Rev.* **2002**, 31, 301.
- [26] J. Xu, L. E. Jarocho, T. Zollitsch, M. Konowalczyk, K. B. Henbest, S. Richert, M. J. Golesworthy, J. Schmidt, V. Déjean, D. J. C. Sowood, M. Bassetto, J. Luo, J. R. Walton, J. Fleming, Y. Wei, T. L. Pitcher, G. Moise, M. Herrmann, H. Yin, H. Wu, R. Bartölke, S. J. Käsehaagen, S. Horst, G. Dautaj, P. D. F. Murton, A. S. Gehrckens, Y. Chelliah, J. S. Takahashi, K.-W. Koch, S. Weber, et al., *Nature* **2021**, 594, 535.
- [27] T. M. D. Alharbi, Y. Shingaya, K. Vimalanathan, T. Nakayama, C. L. Raston, *ACS Appl. Nano Mater.* **2019**, 2, 5282.
- [28] S. Costa, E. Borowiak-Palen, M. Kruszynska, A. Bachmatiuk, R. J. Kalenczuk, *Mater. Sci.-Poland* **2008**, 26, 433.
- [29] X. Luo, P. Smith, C. L. Raston, W. Zhang, *ACS Sustain. Chem. Eng.* **2016**, 4, 3905.
- [30] K. Vimalanathan, Z. Zhang, J. Zou, C. L. Raston, *Chem. Commun.* **2023**, 59, 9698.
- [31] I. K. Alsulami, T. M. D. Alharbi, D. P. Harvey, C. T. Gibson, C. L. Raston, C. L., *Chem. Commun.* **2018**, 54, 7896.
- [32] T. M. D. Alharbi, Q. Li, C. L. Raston, *ACS Sustainable Chem. Eng.* **2021**, 9, 16044.
- [33] C. Bonizzoni, A. Ghirri, F. Santanni, *Quantum Inform.* **2024**, 10, 41.